Direct laser welding of a Cr-Si alloyed coating-free press-hardened steel

Qing Zhou, Zhao Li, Lingyu Wang† and Wei Xu

State Key Laboratory of Rolling and Automation, Northeastern University, Shenyang, Liaoning 110819, China
†E-mail: wanglingyu@ral.neu.edu.cn
www.neu.edu.cn

Luning Wang and Fei Wang

Technical Center of Ben Gang Group Corporation, Ben Gang Group Corporation Co. Ltd., Benxi, Liaoning 117021, China
www.bxsteel.com

The Al-Si-coated 22MnB5 steel used for press hardening is a pivotal lightweight material for advancing automotive weight reduction and safety standards. However, the formation of brittle δ-ferrite in the Al-Si coating during welding reduces the mechanical performance of the weld. In this investigation, a pioneering high-temperature oxidation-resistant press hardened steel was demonstrated to enable ablation-free laser welding. Laser welding and hot stamping tests were conducted at various power settings while maintaining a constant welding speed. The influence of laser power on microstructure and mechanical properties were investigated. Results show uniform strength and improved mechanical properties after thermal forming. This study advances high-quality laser welding for thermoplastic forming steel, optimizing efficiency and offering valuable insights for practical deployment.

Keywords: Coating-free; Press hardened steel; Direct laser welding; Weld microstructures.

1. Introduction

With the escalating energy crisis and environmental pollution, energy conservation and emissions reduction have emerged as paramount development priorities in the automotive industry. The reduction of vehicle weight stands out as a crucial avenue toward achieving energy efficiency and emissions reduction[1-3]. The utilization of high-strength steels in automobile manufacturing not only reduces the overall weight of the vehicle structure but also enhances automotive safety. Nevertheless, traditional cold-formed high-strength steel exhibits certain drawbacks, including substantial springback and die wear[4, 5]. The tensile strength of press hardened steels can exceed 1500 MPa, offering advantages such as high precision and minimal springback[6, 7]. Hence, it finds widespread application in the manufacturing of critical structural components such as anti-collision beams and A-pillars[8]. At present, 22MnB5 is the most commonly employed press-hardened steel. To mitigate surface oxidation problem during hot stamping processes, Al-Si coatings are extensively utilized in press hardened steels[9-11]. During laser welding of Al-Si-coated press-hardened steels, aluminum from the coating can infiltrate the weld, leading to Al

Y. Zhang and M. Ma (eds.), *Proceedings of the 7th International Conference on Advanced High Strength Steel and Press Hardening (ICHSU 2024)*, Atlantis Highlights in Materials Science and Technology 3,
https://doi.org/10.2991/978-94-6463-581-2_73

enrichment and consequently influencing the microstructure and mechanical properties of the weld[12]. Sun et al.[13] investigated the impact of Al-Si coating on the microstructure of laser welding in 22MnB5 steel. It revealed that an elevated Al content in the melt pool resulted in the formation of a greater number of delta-ferrite phases, which is detrimental for component safety. The current removal method for Al-Si coatings cannot meet the requirements of industrial production and the ablation methods are strictly protected by proprietary patents[14], which further raises the overall cost of the welding process.

Recently, a coating-free press hardened steel (CF-PHS) was developed to address the abovementioned issues. The CF-PHS has Cr and Si additions that provide good oxidation resistance during the press hardening process, eliminating the need for any additional coatings. This paper introduces a new method for direct press hardening of 1500 MPa-grade CF-PHS steel after laser welding without the need to strip the coating. The macroscopic morphology and microstructure of the base metal (BM), heat-affected zone (HAZ), and fusion zone (FZ) before and after press hardening were characterized. The mechanical properties of the joints were also evaluated. The changes in the microstructure and properties of the welded joints before and after press hardening were elucidated, providing a theoretical basis for the wide application of CF-PHS in practical production.

2. Experimental procedure

The experiment employed the CF-PHS provided by Benxi Iron & Steel (Benxi, China) with a thickness of 1.9 mm. The chemical composition of the steel is presented in Table 1.

Table 1. Chemical composition of the CF-PHS (wt. %).

C	Mn	Si	Cr	Nb	Fe
0.21	1.34	⩽2.00	⩽2.50	0.027	Bal.

The schematic diagram of laser welding is illustrated in Fig. 1. For the laser welding experiment, the selected laser welder was HS-CM-3000-C-G2 (Han's Yueming Laser Group, China), featuring a laser wavelength of 1080 nm, a spot size of 100 μm, a focusing mirror with a focal length of 200 mm, a defocus of 15 mm, and a protective gas (Ar) flow rate of 20 mL/min. Table 2 provides the parameters for the welding tests.

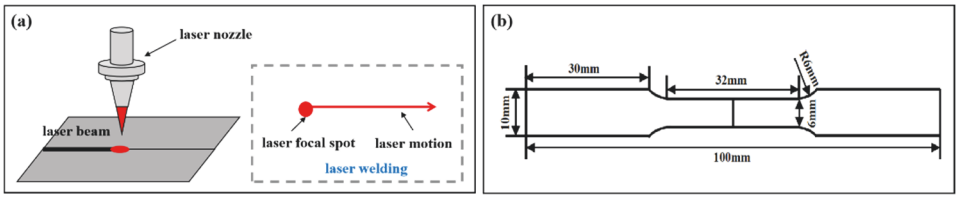

Fig. 1. (a) Schematic diagram of laser welding; (b) Schematic diagram of tensile specimen dimensions.

Table 2. Welding Parameters used in the current study.

No.	Laser power (W)	Welding speed (m min−1)
1	3000	4.2
1	4000	4.2
3	5000	4.2
4	6000	4.2

After laser welding, the blanks underwent heating and was held for 340 seconds at 930°C in a furnace to achieve full austenitization during press hardening. Subsequently, the blanks were rapidly transferred to a flat die, with a press duration of 12 seconds.

To ensure the central positioning of the weld, the dimensions of the tensile specimens are illustrated in Fig. 1(b). The tensile tests were conducted at ambient temperature and a tensile velocity of 2 mm/min. The microhardness of the specimen, subjected to a load of 1kg, was assessed using a micro-Vickers hardness tester for a duration of 10 seconds. Ultimately, the microstructures were examined using an Olympus DSX 510 optical microscope (OM) and a Carl Zeiss Ultra Plus field emission scanning electron microscope (FEG-SEM).

3. Results and Discussion

3.1. *Microstructural characterization of the weld*

The cross-sectional morphology of the laser welding joint of CF-PHS before press hardening is shown in Fig. 2. It can be seen from Fig. 2 that both the upper and lower surfaces of the FZ are concave after laser welding, and the cross-sectional shape is a "dumbbell" shape with a wide upper and lower part and a narrow middle part, with clear boundaries between the FZ, the HAZ, and the BM. When the laser speed is 4.2 m/min, with the increase of welding power, the heat input value also increases, resulting in a wider welding zone. From Fig. 2, it can be observed that the weld collapse is smaller at laser powers of 5 kW and 6 kW compared to 3 kW and 4 kW. Better weld formation can be achieved at higher laser powers but the quality of the weld should be okay at lower laser powers.

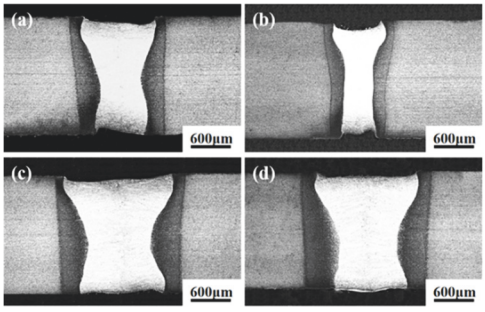

Fig. 2. Cross-sectional morphology of the weld joint before press hardening: (a) 3 kW; (b) 4 kW; (c) 5 kW; (d) 6 kW.

Fig. 3(a) depicts the optical micrograph of the laser-welded joint before press hardening, taken as an example with a laser power of 6 kW. Fig. 3(b) shows the microstructure of the BM, mainly consisting of ferrite and carbides. Fig. 3(c) illustrates the microstructure of the HAZ. During laser welding, due to the thermal conduction effect of the joint, the peak heating temperature in the HAZ is higher than the austenite transformation temperature (Ac3) but lower than the melting temperature of the BM. The microstructure undergoes complete austenite decomposition, resulting in a final structure of bainite and tempered martensite. Fig. 3(d) displays the microstructure of the FZ. As the steel is melted and then rapidly cooled to below the Ms point at a speed greater than the critical cooling rate, the microstructure is mainly martensite, with minimal carbides.

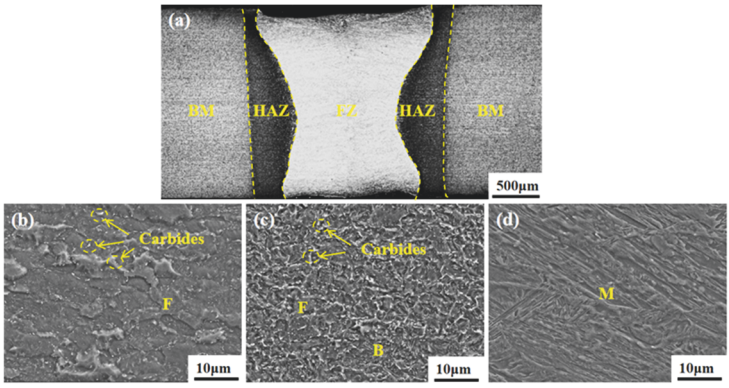

Fig. 3. Microstructure of welded joint before press hardening taken from the sample welded using a laser power of 6 kW: (a) Overview of the weld joint; (b) BM; (c) HAZ; (d) FZ.

Fig. 4 shows the cross-sectional morphology of the laser-welded joint of the CF-PHS after press hardening. To facilitate subsequent mechanical property testing, the welding test plates were polished in advance to remove the oxide layer. It can be observed from Fig. 4 that the cross-sectional shape of the FZ after press hardening remains a "dumbbell" shape with wider upper and lower parts and a narrower middle part. However, the boundaries between the FZ, the HAZ, and the BM are no longer distinct after press hardening.

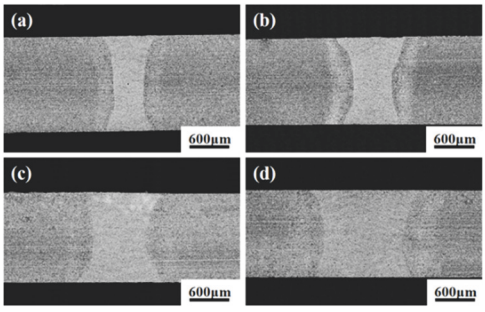

Fig. 4. Cross-sectional morphology of the weld joint after press hardening: (a) 3 kW; (b) 4 kW; (c) 5 kW; (d) 6 kW.

Fig. 5(a) shows the optical micrograph of the laser-welded joint after press hardening, taken as an example with a welding power of 6 kW. Fig. 5(b) and Fig. 5(c) displays the microstructure of the BM and the HAZ, which have also largely transformed into martensite. Both BM and HAZ has remaining carbide within the them as the heating process during press hardening is unable to dissolve all alloy carbides as demonstrated in our previous works[15, 16]. Fig. 5(d) presents the microstructure of the FZ, primarily consisting of martensite with no visible carbides as the laser welding process has already eliminated them as shown in Fig. 3(d). The entire welded joint exhibits uniform microstructure, with no evidence of ferrite softening phase.

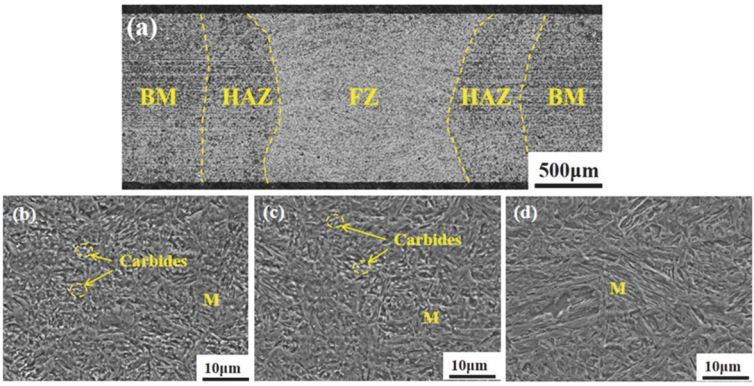

Fig. 5. Microstructure of welded joint after press hardening taken from the sample welded using a laser power of 6 kW: (a) Overview of the weld joint; (b) BM; (c) HAZ; (d) FZ.

3.2. *Mechanical properties of the weld*

Fig. 6(a) illustrates the hardness profile of the welded joint before press hardening, while Fig. 6(b) depicts the hardness profile after press hardening. In Fig. 6(a), the hardness of the welded joint increases from the BM to the HAZ and then to the FZ, with no local softening observed. The BM exhibits a hardness of approximately 210 HV, while the weld registers around 520 HV. In Fig. 7(b), the hardness of the welded joint press hardening demonstrates overall improvement and becomes more uniform. The BM reaches about 520 HV, and the weld measures around 540 HV, with the weld hardness slightly surpassing that of the BM. Across the laser power range of 3 kW to 6 kW, different welding powers exhibit no significant impact on the hardness of the welded joints before and after press hardening.

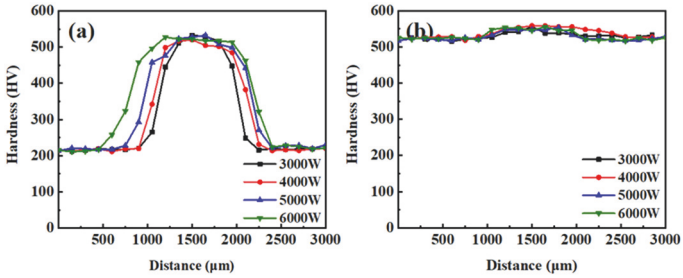

Fig. 6. Hardness of welded joint: (a) before press hardening; (b) after press hardening.

Fig. 7(a) presents the tensile curves of the welded joint before press hardening, while Fig. 7(b) depicts the tensile curves after press hardening. In Fig. 7(a), the yield strength of the welded joint before press hardening is approximately 500 MPa, the tensile strength is about 700 MPa, and the elongation reaches about 18%. Conversely, in Fig. 7(b), the yield strength of the welded joint after press hardening significantly increases to around 1300 MPa, the tensile strength rises to approximately 1600 MPa, and the elongation decreases to about 8%. Fig. 8 shows tensile fracture position of welded samples. From Fig. 8, it can be seen that regardless of whether it is before or after press hardening, the failure position of the laser-welded plate with transverse welds is on the BM, indicating that the welding process and parameters selected in this study are reasonable, and the welding quality is qualified.

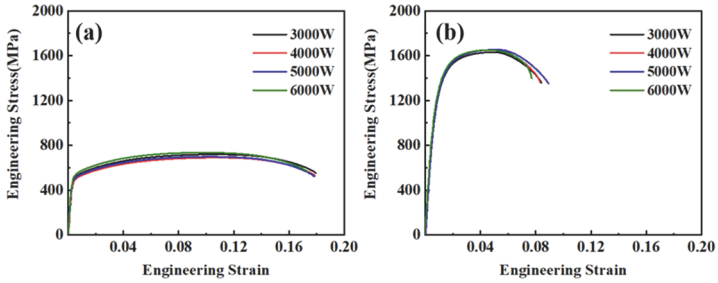

Fig. 7. Tensile curves of welded joint: (a) before press hardening; (b) after press hardening.

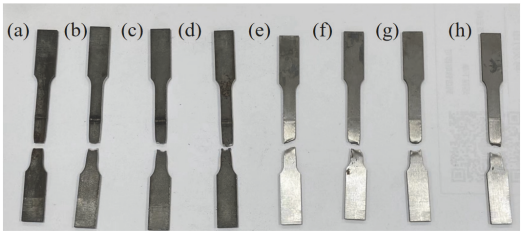

Fig. 8. Tensile fracture position of welded samples: (a) - (d) 3 kW - 6 kW, before press hardening; (e) - (f) 3 kW - 6 kW, after press hardening.

4. Conclusion

In this study, laser welding and subsequent press hardening experiments were conducted on CF-PHS laser-welded plates at the same welding speed but with different welding powers. It was found that the laser-welded joints of CF-PHS plates could be welded directly and exhibited good strength. When the welding power was between 3 kW and 6 kW, the weld width increased with the increase in welding power. Within this welding process window, all the properties of CF-PHS laser-welded plates remained at an excellent level. They are expected to replace Al-Si coated plates and be widely used in practice.

Acknowledgments

The authors thank the help from the Han's Yueming Laser Group for laser welding.

References

1. A, K., Developing lightweight concepts in the automotive industry: taking on the environmental challenge with the SaNätt project. Journal of Cleaner Production, 2014. 66(66): p. 337-346.
2. T, S., Physical metallurgy of modern high strength steel sheets. ISIJ International, 2001. 41(6): p. 520-532.
3. Aggeri, F., M. Elmquist, and H. Pohl, Managing learning in the automotive industry – the innovation race for electric vehicles. International Journal of Automotive Technology and Management, 2009. 9(2).
4. Huang, F., et al., Automotive Steel with a High Product of Strength and Elongation used for Cold and Hot Forming Simultaneously. Materials, 2021. 14(5).
5. Li, S.S. and H.W. Luo, Medium-Mn steels for hot forming application in the automotive industry. International Journal of Minerals Metallurgy and Materials, 2021. 28(5): p. 741-753.
6. Karbasian, H. and A.E. Tekkaya, A review on hot stamping. Journal of Materials Processing Technology, 2010. 210(15): p. 2103-2118.
7. Taylor, T. and A. Clough, Critical review of automotive hot-stamped sheet steel from an industrial perspective. Materials Science and Technology, 2018. 34(7): p. 809-861.
8. Hein, P. and J. Wilsius, Status and innovation trends in hot stamping of USIBOR 1500 P. Steel Research International, 2008. 79(2): p. 85-91.
9. Siltanen, J., A. Minkkinen, and S. Jarn, Laser welding of coated press-hardened steel 22MnB5. 16th Nordic Laser Materials Processing Conference, Nolamp16, 2017. 89: p. 139-147.
10. Fan, D.W. and B.C. De Cooman, State-of-the-Knowledge on Coating Systems for Hot Stamped Parts. Steel Research International, 2012. 83(5): p. 412-433.
11. Wang, Z., et al., Improving the bending toughness of Al-Si coated press-hardened steel by tailoring coating thickness. Scripta Materialia, 2021. 192: p. 19-25.
12. Ehling W, C.L., Pic A, et al., Development of a laser decoating process for fully functional Al-Si coated press hardened steel laser welded blank solutions. Proceedings of 5th International WLT-conference on Lasers in Manufacturing, Munich, 2009: p. 409-413.
13. Sun, Q., et al., Suppression of δ-ferrite formation on Al-Si coated press-hardened steel during laser welding. Materials Letters, 2019. 245: p. 106-109.
14. Messaoudi H, M.S., Tromenschläger W, Picosecond laser cleaning of hot stamped 22MnB5 steel. 2017. 5: p. 504-508.
15. Wei, X., et al., Cr-alloyed novel press-hardening steel with superior combination of strength and ductility. Materials Science and Engineering: A, 2021. 819.
16. Chai, Z., et al., Cr-enriched carbide induced stabilization of austenite to improve the ductility of a 1.7 GPa−press-hardened steel. Scripta Materialia, 2023. 224.